A Novel Modified Control Scheme in Grid-Tied Photovoltaic System for Power Quality Enhancement

Babu, Narendra P.; Guerrero, Josep M.; Siano, Pierluigi; Peesapati, Rangababu; Panda, Gayadhar

Published in:
IEEE Transactions on Industrial Electronics

DOI (link to publication from Publisher):
10.1109/TIE.2020.3031529

Publication date:
2021

Document Version
Accepted author manuscript, peer reviewed version

A Novel Modified Control Scheme in Grid-tied Photovoltaic System for Power Quality Enhancement

Narendra Babu P[1], Josep M. Guerrero[2], *Fellow, IEEE*, Pierluigi Siano[3], *SM, IEEE*, Ranga Babu Peesapati[4], *M, IEEE* and Gayadhar Panda[1], *SM, IEEE*

***Abstract*—In this article, a modified reduced order generalized integrator based frequency locked loop (MROGI-FLL) is proposed for controlling the interfacing inverter of the grid-tied photovoltaic (PV) system to mitigate the harmonics. Additionally, a fuzzy tuned PID (FPID) controller is integrated in the proposed scheme to minimize the steady-state error which results the voltage level is maintained constant at the common dc-link bus terminals. The MROGI-FLL is designed to evaluate the three-phase reference currents by extracting the fundamental constituents from the load currents and grid voltages. The proposed MROGI-FLL have several advantages such as better harmonic mitigation capability, control adaptivity, adaptive frequency and phase, grid synchronisation and low computation burden. The proposed reference current generator is simulated on matlab/simulink platform under steady-state and various transient conditions.The comparative study of proposed scheme is compared with the existing and adaptive control techniques which assures the potency of the proposed control algorithm in-terms of harmonic mitigation, dc-offset rejection, frequency variation and computation burden. Finally, the experimental results are verified through an experimental platform by using the dSPACE evaluation kit and both the simulation and hardware characteristics are well justified to the IEEE-519 standard limits.**

***Index Terms*—Active power filter, FLL, FPID, MROGI, power quality, PV system, ROGI, THD.**

I. Introduction

Renewable energy systems struggle with quality of power issues due to current and voltage harmonics generated from power electronics devices with their non-linear switching characteristics. The appearance of harmonics minimizes the life extent and give raises to malfunction of the apparatus that are connected to the network. So, the reactive power compensation and harmonic elimination are important requirements and determine great research attention [1]. Traditionally, passive filters (PF) are utilized for harmonics reduction, however they exhibit some drawbacks such as huge size, resonance problems and fixed filtering features. So in order to overwhelm the above drawbacks, active power filters (APF) are introduced [2],[3]. APFs are more capable in eliminating current and voltage harmonics. They are mainly classified into two types, *i.e.*, shunt APF and series APF. Shunt APFs are used to eliminate the harmonics of the current and series APFs are utilized to eliminate the harmonics of the voltage.

In order to enrich the quality of electrical power, different linear and nonlinear control approaches are implemented in APFs system [4-8]. During the definition of system variables, controller is designed based on a robust control approach, computational complexity and automatic adaption. In the last two decades, numerous control approaches have been implemented for APF, such as instantaneous reactive power theory (IRP) [9], synchronous reference frame (SRF) theory [10], fryze current compensation theory [11], ADALINE (Adaptive linear element) based techniques, neural network techniques [12], Kalman filter based techniques [13], wavelet transform [14], discrete Fourier transform techniques [15]. The IRP theory cannot provide satisfactory results during unbalance and distorted conditions. The SRF theory also have poor performance under dynamic condition because of low pass filter. Although the fryze and ADALINE approaches have good performances under steady state and dynamic conditions, they provide poor performance at distorted grid condition. During system frequency variation, neural network techniques suffer with proper learning. Kalman filter based techniques, wavelet transform, and discrete Fourier transform techniques are failed to improving the system dynamic performance under grid transient conditions [9-15].

Moreover various adaptive control approaches, such as recursive least square (RLS) [16], least mean square (LMS) [17], least mean fourth (LMF) [18], improved linear sinusoidal tracer [ILST] [19], variable step size least mean square (VSS-LMS) [20], and adaptive notch filter [ANF] [21] have been researched in recent years. However they have some draw-

Manuscript received January 28, 2020; revised July 05, 2020 and September 10, 2020; accepted October 04, 2020. This work was supported in part by the RECTPCL-CSR Funded Project under Grant RECTPCL/CSR/2016-17/693 and VILLUM FONDEN under the VILLUM Investigator Grant (no. 25920): Center for Research on Microgrids (CROM); www.crom.et.aau.dk. (*Corresponding author: Narendra Babu P*).

Narendra Babu P and Gayadhar Panda are with the Electrical Engineering Department, National Institute of Technology Meghalaya, Shillong-793003, Meghalaya, India (e-mail: narem.perumal@nitm.ac.in and gayadhar.panda@nitm.ac.in).

J. M. Guerrero is with the Center for Research on Microgrids (CROM), Department of Energy Technology, Aalborg University, 9220 Aalborg East, Denmark (e-mail: joz@et.aau.dk).

P. Siano is with the Department of Management and Innovation Systems, University of Salerno, 84084 Fisciano, Italy (e-mail: psiano@unisa.it).

Rangababu Peesapati is with the Electronics and communication Engineering Department, National Institute of Technology Meghalaya, Shillong-793003, Meghalaya, India (e-mail: p.rangababu@nitm.ac.in).

This article has been accepted for publication in a future issue of this journal, but has not been fully edited. Content may change prior to final publication. Citation information: DOI 10.1109/TIE.2020.3031529, IEEE Transactions on Industrial Electronics

backs, such as those related to the tracking of the steady state response that is not adequate due to the 4th order optimization, high complexity, high computational burden and low weight convergence rate.

Thus, to design a robust controller, the artificial intelligence field has been investigated. The potential of these adaptive control techniques are learning, self adaptive and self organizing. The echo state network (ESN) approach one type of recurrent neural network (RNN) approach which is found appropriate for fundamental weight extraction from nonlinear load currents. It also has excellent dynamic response for real-time applications and for the closed loop systems [22]. However, the above-said controllers are not preferable if considering the dc-offset rejection and grid synchronization. In order to overcome the above difficulties, very recently, few generalized integrator (GI) based adaptive control schemes have been developed in the literature. Moreover, frequency locked loop (FLL) based control schemes have collected more attenuation in various power and energy applications for grid synchronization, power signal decomposition and electrical motor control.

In this work, we focused on modification of conventional reduced order generalized integrator (ROGI) based FLL (ROGI-FLL) which is also called as complex band-pass filter (CBF) based FLL (CBF-FLL) [23],[24]. The conventional ROGI based FLL control structure is shown in Fig. 2. In the ROGI based FLL structure, a first order (FO) CBF (FO-CBF) is perceived by employing the ROGI based unity feedback control loop. The ROGI based FLL control scheme separates the load current fundamental constituent (FC) and also estimate the fundamental frequency (FF) by employing the FLL control scheme. In recent years, few advanced control techniques have been introduced to enrich the ROGI based FLL filtering ability, implementing more centered parallel ROGIs at the frequency disturbances [23],[26]. The in-loop filter (ILF) control scheme is designed for FLL with more filtering ability [27]. Based on this control structure, the disturbance mitigation ability can be improved by incorporating the band pass filter (BPF) in the control loop. In the ROGI-FLL pre-filtering stage, more FO-CBFs has been employed to change the frequency by utilizing the feedback frequency loop has been developed in [28],[29]. In this paper, a modified ROGI-FLL is developed to enrich the performance of the system by utilizing the complex control gain. The modification of the proposed control scheme is a cross connecting between α β signals. The modified control algorithm is shown in Fig. 3. The stability analysis of the MROGI with existed ROGI control schemes is shown in Fig. 4 which assures the effectiveness of the proposed control scheme in-terms of dc-offset rejection. The existing control techniques simulated in MATLAB and using experimental platforms, have demonstrated a higher execution time than the proposed technique that thus exhibits lower computational complexity. The distinctive characteristics of the modified control scheme are as follows.

- The proposed adaptive modified ROGI-FLL control scheme is employed to extract the FC from the load currents and grid voltages; consequently, it generates the anti-harmonic currents by using the PWM controller.
- The modified cross-coupling in the proposed control scheme is utilized to evaluate the amplitude, frequency and phase angle with adaptive basis.
- The proposed method is based on a better understanding between damping and speed of the FLL's transient response which gives a better dynamic performance with very small overshoot by modifying the control scheme.
- The feed-forward constituent of the PV system is integrated into the control structure to enrich the dynamic behaviour of the system.
- The adaptive fuzzy tuned PID (FPID) controller is integrated into the proposed scheme to minimize the steady-state error and maintaining the voltage level at the common dc-link bus terminals.
- Comparison of the proposed control technique with few conventional as well as other recently developed control techniques is performed. The necessity of developing an adaptive control strategy for power quality enhancement and clean power conversion is justified by considering grid perturbations and load disturbances.

II. Grid-tied photovoltaic system description

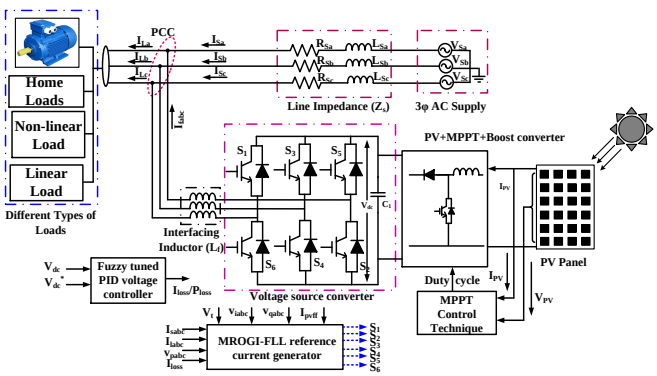

Fig. 1. Block diagram of grid connected PV system with proposed control scheme

Fig. 1 shows the considered grid-tied photovoltaic (PV) system power stage and the implementation of the proposed control technique. The overall system consists of two-stage PV system feeding power to the grid. Incremental conductance MPPT control technique is used for maximum power tracking and a boost converter is carefully designed taking proper DC-bus capacitor design. It is presumed that the boost converter works under continuous conduction (CC) mode with high switching frequency. So that, the inductor size and cost is reduced. The DC loads can be optionally connected to the common DC-bus. The FPID controller ensures ripple free DC-bus voltage and it is combined with the FC of the load current generated using proposed reference current generation technique to generate the reference currents for controlling the APF inverter [30][31]. A PMW current controller generates the required switching signals for the APF. To filter out the high order harmonics, a filter inductor is connected between the APF and the AC bus. Various types of linear and non-linear loads can be connected along with the utility grid to the common AC bus. The proposed grid-tied system in this

This article has been accepted for publication in a future issue of this journal, but has not been fully edited. Content may change prior to final publication. Citation information: DOI 10.1109/TIE.2020.3031529, IEEE Transactions on Industrial Electronics

work is connected to a linear resistive-inductive load and an uncontrolled rectifier which acts as non-linear load.

III. Proposed Control Scheme

The conventional control schematic of ROGI is shown in Fig. 2. The modelling of modified ROGI control scheme is obtained by adding the red lines blocks in Fig. 3. The modified ROGI control scheme's mathematical analysis is expressed as follows.

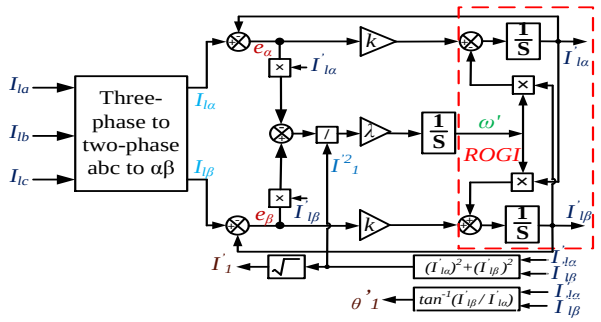

Fig. 2. Conventional ROGI control structure

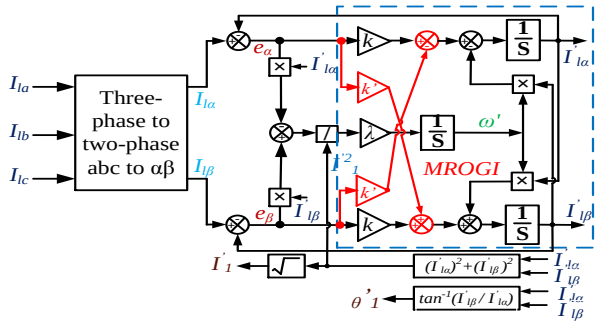

Fig. 3. Modified ROGI control structure

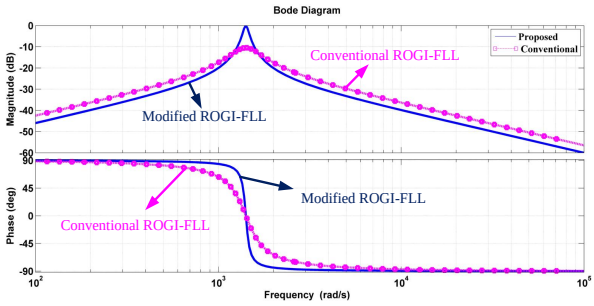

Fig. 4. Stability analysis of modified ROGI-FLL with traditional ROGI by using (17) and (18)

$$\frac{dI_{l\alpha}^{'}}{dt} = -\omega^{'} I_{l\beta}^{'} + k(I_{l\alpha} - I_{l\alpha}^{'}) - k^{'}(I_{l\beta} - I_{l\beta}^{'}) \tag{1}$$

$$\frac{dI_{l\beta}^{'}}{dt} = \omega^{'} I_{l\alpha}^{'} + k(I_{l\beta} - I_{l\beta}^{'}) + k^{'}(I_{l\alpha} - I_{l\alpha}^{'}) \tag{2}$$

$$\begin{cases} \frac{d\omega^{'}}{dt} = \frac{\lambda}{I_1^{'2}}[I_{l\alpha}^{'}(I_{l\beta} - I_{l\beta}^{'}) - I_{l\beta}^{'}(I_{l\alpha} - I_{l\alpha}^{'})] \\ = \frac{\lambda}{I_1^{'2}}[I_{l\alpha}^{'} I_{l\beta} - I_{l\beta}^{'} I_{l\alpha}] \end{cases} \tag{3}$$

$$\theta_1^{'} = tan^{-1}(\frac{I_{l\beta}^{'}}{I_{l\alpha}^{'}}) \tag{4}$$

$$I_1^{'} = \sqrt{I_{l\alpha}^{'2} + I_{l\beta}^{'2}} \tag{5}$$

where $I_{l\alpha}^{'}$ and $I_{l\beta}^{'}$ are the α β FC extraction of the load currents, 'k' is the controller gain, k$^{'}$ is the modified controller gain, e_α and e_β are the α β error currents of the load current, $I_{l\alpha}$ and $I_{l\beta}$ are the α β constituents of the load current, λ is the integral gain of the controller, $\theta_1^{'}$ is the estimated phase angle, $I_1^{'}$ is the estimated current amplitude and $\omega^{'}$ is estimated frequency. The cross coupling gain term (kÂ´) is calculated by using the equation as k'= ωL. The Lambda (λ) is chosen as an integral term gain high enough to get good tracking performance, trading off with the stability of the system and the gain k is assumed as 0.707 [32]. For tuning the parameters of the proposed control scheme, a linear quadratic regulation (LQR) method [32] is used.

The proposed control scheme has been split into four stages such as frequency, phase angle, amplitude tracking and reference current calculation. The mathematical analysis for designing the four stages is given in further subsections.

A. Stage I: Frequency Tracking

By using (3), we can written as

$$\begin{cases} \frac{d\omega^{'}}{dt} = \frac{\lambda I_1 I_1^{'}}{I^{'2}}[cos(\theta_1^{'})sin(\theta_1) - sin(\theta_1^{'})cos(\theta_1)] \\ = \frac{\lambda I_1}{I_1^{'}}[sin(\theta_1 - \theta_1^{'})] \end{cases} \tag{6}$$

Let us assume that $\theta_1^{'} \approx \theta_1$ and $I_1^{'} \approx I_1$, therefore (6) can be written as

$$\frac{d\omega^{'}}{dt} \approx \lambda(\theta_1 - \theta_1^{'}) \tag{7}$$

$$\frac{d \triangle \omega^{'}}{dt} \approx \lambda(\triangle\theta_1 - \triangle\theta_1^{'}) \tag{8}$$

where $\triangle\omega^{'}$ represents the change in frequency, $\triangle\theta_1^{'}$ and $\triangle\theta_1$ represents the change in phase angle respectively.

B. Stage II: Phase Angle Tracking

The phase angle tracking is obtained by differentiating (4) with respect to the time, which can be written as

$$\frac{d\theta_1^{'}}{dt} = \frac{I_{l\alpha}^{'}\frac{dI_{l\beta}^{'}}{dt} - I_{l\beta}^{'}\frac{dI_{l\alpha}^{'}}{dt}}{I_{l\alpha}^{'2} + I_{l\beta}^{'2}} = \frac{I_{l\alpha}^{'}\frac{dI_{l\beta}^{'}}{dt} - I_{l\beta}^{'}\frac{dI_{l\alpha}^{'}}{dt}}{I_1^{'2}} \tag{9}$$

Substitute (1) and (2) in (9), we get

$$\frac{d\theta_1^{'}}{dt} = \frac{\begin{array}{r}\omega^{'}[I_{l\alpha}^{'2} + I_{l\beta}^{'2}] + k[I_{l\alpha}^{'}(I_{l\beta} - I_{l\beta}^{'}) - I_{l\beta}^{'}(I_{l\alpha} - I_{l\alpha}^{'})] \\ + k^{'}[I_{l\alpha}^{'}(I_{l\alpha} - I_{l\alpha}^{'}) - I_{l\beta}^{'}(I_{l\beta} - I_{l\beta}^{'})]\end{array}}{I_1^{'2}} \tag{10}$$

$$\begin{cases} \frac{d\theta_1^{'}}{dt} = \omega^{'} + \frac{k}{\lambda}\frac{d\omega^{'}}{dt} + \frac{k^{'}}{I_1^{'2}}[I_1 I_1^{'} cos(\theta_1 - \theta_1^{'}) - I_1^{'2}] \\ \approx \omega^{'} + \frac{k}{\lambda}\frac{d\omega^{'}}{dt} + \frac{k^{'}}{I_1^{'}}[I_1 - I_1^{'}] \end{cases} \tag{11}$$

Therefore,

$$\frac{d \triangle \theta_1^{'}}{dt} \approx \triangle\omega^{'} + \frac{k}{\lambda}\frac{d \triangle \omega^{'}}{dt} + \frac{k^{'}}{I_m}[\triangle I_1 - \triangle I_1^{'}] \tag{12}$$

This article has been accepted for publication in a future issue of this journal, but has not been fully edited. Content may change prior to final publication. Citation information: DOI 10.1109/TIE.2020.3031529, IEEE Transactions on Industrial Electronics

where $\triangle\omega^{'}$ represents the change in frequency, $\triangle\theta_1^{'}$ and $\triangle\theta_1$ represents the change in phase angle, $\triangle I_1$ and $\triangle I_1^{'}$ represents the change in current respectively.

C. Stage III: Amplitude Tracking

The amplitude tracking is obtained by differentiating (5) with respect to the time, which can be written as

$$\frac{dI_1^{'}}{dt} = \frac{I_{l\alpha}^{'}\frac{dI_{l\alpha}^{'}}{dt} + I_{l\beta}^{'}\frac{dI_{l\beta}^{'}}{dt}}{I_1^{'}} \tag{13}$$

Substitute (1) and (2) in (13), we get

$$\frac{dI_1^{'}}{dt} = \frac{\begin{array}{c}-k^{'}[I_{l\alpha}^{'}(I_{l\beta}-I_{l\beta}^{'}]-I_{l\beta}^{'}(I_{l\alpha}-I_{l\alpha}^{'})] \\ +k[I_{l\alpha}^{'}(I_{l\alpha}-I_{l\alpha}^{'})+I_{l\beta}^{'}(I_{l\beta}-I_{l\beta}^{'})]\end{array}}{I_1^{'}} \tag{14}$$

Therefore (14) can be rewritten as

$$\begin{cases}\frac{dI_1^{'}}{dt} = -\frac{k^{'}I_1^{'}}{\lambda}\frac{d\omega^{'}}{dt} + \frac{k}{I_1^{'}}[I_1 I_1^{'}cos(\theta_1-\theta_1^{'}) - I_1^{'2}] \\ \approx -\frac{k^{'}I_1^{'}}{\lambda}\frac{d\omega^{'}}{dt} + k[I_1 - I_1^{'}]\end{cases} \tag{15}$$

Differentiating (15) change in current with respect to time, we get

$$\frac{d\triangle I_1^{'}}{dt} \approx -k^{'}I_m[(\triangle\theta_1 - \triangle\theta_1^{'})] + k[(\triangle I_1 - \triangle I_1^{'})] \tag{16}$$

The transfer functions of conventional ROGI and modified ROGI for extracting the fundamental constituents from the load currents is expressed as follows

$$Q_{ROGI-FLL}(s) = \frac{I_{l\alpha}^{'}(s)+jI_{l\beta}^{'}(s)}{I_{l\alpha}(s)+jI_{l\beta}(s)} = \frac{k}{(s-j\omega^{'})+k} \tag{17}$$

$$Q_{MROGI-FLL}(s) = \frac{I_{l\alpha}^{'}(s)+jI_{l\beta}^{'}(s)}{I_{l\alpha}(s)+jI_{l\beta}(s)} = \frac{k+jk^{'}}{(s-j\omega^{'})+k+jk^{'}} \tag{18}$$

D. Stage IV: Reference Current Generation

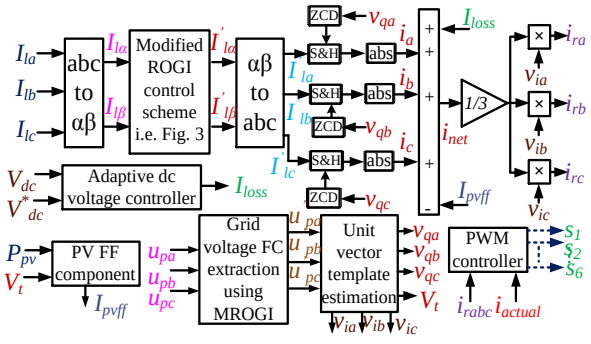

Fig. 5. Complete control schematic of the proposed system

The proposed algorithm's complete control schematic is given in Fig. 5. The FC extraction of the load current and grid voltages, the PV feed forward ($_{pvff}$) and unit vector template (UVT) are required. The UVT is calculated by sensing the grid voltages at the point of common coupling, which is expressed as

$$V_t = \sqrt{0.666(v_{pa}^2 + v_{pb}^2 + v_{pc}^2)} \tag{19}$$

where v_{pa}^2, v_{pb}^2 and v_{pc}^2 are the sensing grid voltages. The quadrature and in-phase UVT constituents of the grid voltages are calculated by using (19).

$$v_{ia} = \frac{v_{pa}}{V_t}, v_{ib} = \frac{v_{pb}}{V_t}, v_{ic} = \frac{v_{pc}}{V_t} \tag{20}$$

where v_{ia}, v_{ib} and v_{ic} are the in-phase constituents of the grid voltages and V_t is the UVT voltage. Therefore, The quadrature UVT constituents of the grid voltages are calculated by using (20), which is expressed as follows.

$$\begin{cases} v_{qa} = \frac{v_{ic}}{1.732} - \frac{v_{ib}}{1.732}, v_{qb} = \frac{1.732.v_{ia}}{2} + \frac{(v_{ib}-v_{ic}).v_{ib}}{3.464}, \\ v_{qc} = -\frac{1.732.v_{ia}}{2} + \frac{(v_{ib}-v_{ic}).v_{ib}}{3.464} \end{cases} \tag{21}$$

An extracted FC from the load currents is sampled and hold at a ZCD unit with UVT quadrature constituents (v_{qa}, v_{qb} and v_{qc}) to generate the active power constituents of the load generated currents (i_a, i_b and i_c). The net constituent of the load currents is calculated by using the PV feed forward term, active power constituents and current loss constituents of the dc link regulator, which is expressed as follows.

$$i_{net} = \frac{i_a + i_b + i_c - I_{pvff} + I_{loss}}{3} \tag{22}$$

The calculated reference currents are obtained by using the fundamental net constituent current (I_{net}) and in-phase UVT constituents v_{ia}, v_{ib} and v_{ic}, which is expressed as follows.

$$i_{ra} = i_{net}.v_{ia}, i_{rb} = i_{net}.v_{ib}, i_{rc} = i_{net}.v_{ic} \tag{23}$$

The calculated reference currents (I_{ra}, I_{rb} and I_{rc}) and actual grid currents (I_{sa}, I_{sb} and I_{sc}) are given to the PWM controller to generate the three phase anti harmonic currents, which are injecting to the utility grid for harmonic mitigation and quality of power enrichment in grid integration PV system.

E. FPID DC voltage regulator

Performance of the traditional P, PI and PID controllers have been found not satisfactory to stable the dc bus voltage during grid and load transient conditions. To bypass the shortcoming, a fuzzy tuned PID adaptive control scheme is designed to calculate the PID gains adaptively during transient conditions [30,31]. The control diagram of the FLPID is shown in Fig. 6. The mathematical modelling of FLPID controller is discussed as follows,

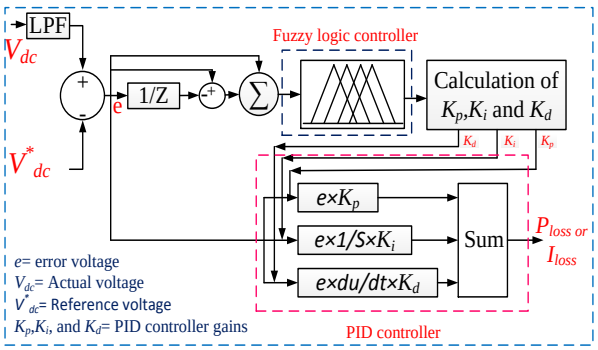

Fig. 6. Schematic diagram of the FLPID voltage controller

$$G_c(s) = k_p + \frac{k_i}{s} + k_d(s) \tag{24}$$

This article has been accepted for publication in a future issue of this journal, but has not been fully edited. Content may change prior to final publication. Citation information: DOI 10.1109/TIE.2020.3031529, IEEE Transactions on Industrial Electronics

$$G_c(s) = k_p(1 + \frac{1}{\frac{k_p}{k_i}(s)} + \frac{k_d}{k_p}(s)) \quad (25)$$

The PID controller's discrete time equivalent equation is

$$u_k = k_p * e(k) + k_i.T_s \sum_{i=1}^{n} e(i) + \frac{k_d}{T_s}.e(k) - e(k-1) \quad (26)$$

where u_k e(k) is the error voltage obtained from the actual and reference dc voltage, is the control signal and T_s is the sampling time.

The mathematical analysis of fuzzy gain scheduling for PID controller is expressed as follows,

$$\begin{cases} k_p^{'} = \frac{k_p - k_{p,min}}{k_{p,max} - k_{p,min}} \\ k_d^{'} = \frac{k_d - k_{d,min}}{k_{d,max} - k_{d,min}} \end{cases} \quad (27)$$

The defuzzification yields are obtained by using the below equations,

$$\begin{cases} k_p^{'} = \sum_{i=1}^{m} \mu_i.k_p^{'}.i \\ k_d^{'} = \sum_{i=1}^{m} \mu_i.k_d^{'}.i \\ \alpha = \sum_{i=1}^{m} \mu_i.\alpha_i \end{cases} \quad (28)$$

The PID controller's gains are obtained by using the below equations,

$$\begin{cases} k_p = (k_{pmax} - k_{pmin}).k_p^{'} + k_{pmin}) \\ k_i = \frac{k_p^2}{\alpha.k_d} \\ k_d = (k_{dmax} - k_{dmin}).k_d^{'} + k_{dmin}) \end{cases} \quad (29)$$

IV. Simulation Analysis

The entire system has been implemented using Matlab/Simulink software platform. The parameters are taken for the proposed system are given in Tables I and II respectively. A grid-connected PV system is examined for power quality improvement at the consumer terminals by using the proposed MROGI-FLL technique under steady state, grid voltage dynamic, load removed, distorted supply voltage and dynamic load state conditions. A comparative study of the MROGI-FLL with conventional techniques is also carried out which are tabulated in Tables III, IV and V respectively.

TABLE I
SPECIFICATIONS OF THE SYSTEM

Specifications	Simulation and Experimental
Grid voltage (V_s)	230V
Grid power (P_s)	6kW
Frequency (f)	50 Hz
Line Impedance (Z_l)	R=0.01Ω, L=1.5mH
Interfacing inductor (L_{apf})	2.2mH
Non-linear load (RL)	50Ω, 40mH
Load power (P_l)	6kW
DC bus capacitor (C_{dc}) [33]	2200μF
DC bus reference voltage	375V
α β constituent gain (k)	0.707
Cross coupling gain ($k^{'}$)	-64
Lambda (λ)	12791
Estimated frequency ($\omega^{'}$)	2×π×f

TABLE II
SPECIFICATIONS OF PV SYSTEM

Specifications	Simulation	Experimental
PV power (P_{pv})	2kW	1.6kW
Irradiation (G)	1000 W/m^2	1000 W/m^2
Open circuit voltage (V_{oc})	210V	200V
Short circuit current (I_{sc})	10.85A	8.96A
Max PV voltage (V_{mp})	190V	190V
Max PV current (I_{mp})	10.52A	8.42A
DC-link voltage (V_dc)	375V	375V
DC-link current (I_dc)	4.3A	4.3A
No. of series modules (N_S)	11	6
No. of parallel modules (N_P)	3	1

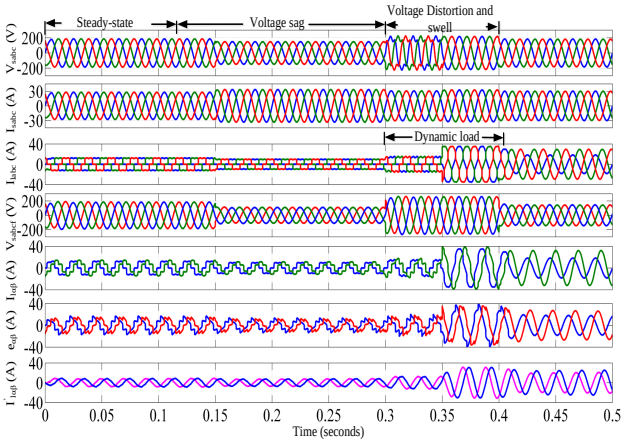

Fig. 7. System characteristics with various test cases

A. Balanced supply voltage condition

The proposed APF scheme's performance is performed under grid voltage balanced condition. Fig. 7 and 8 displays the simulation results under steady-state, voltage fall-raise, A-phase load disconnected, increased load, voltage distorted and unbalanced conditions. In Fig. 7, from 0 to 0.15s, the system operates with balanced supply voltage condition. Before compensation, the THD content in the grid currents is 29.96%. After compensation, the source current becomes more close to sinusoidal wave and the THD in the grid current decreases to 2.162%. In this case, the PV supply is maintained constant and better performance of the APF is achieved using the proposed control technique. Fig. 7 shows the three-phase source voltages (V_{sabc}), and source currents in all three-phases (I_{sabc}), load currents (I_{labc}), extracted grid voltages (V_{sabcf}), load α β components ($I_{l\alpha\beta}$), α β error components $e_{\alpha\beta}$), FC extraction of load currents ($I_{l\alpha\beta}$f). Fig. 8 displays the control characteristics of the proposed systems which displays the net load current (I_{net}), unit-vector template voltage (V_t), in-phase and quadrature voltage constituents (V_{iabc} and V_{qabc}), the reference currents in all three-phases (I_{rabc}), anti-harmonic current of all phases and the dc-bus voltage (V_{dc}). The proposed control performance under this condition is well justified and the THD of the source current is found within the IEEE-519 limits.

B. Grid voltage sag-swell condition

The proposed PV integrated shunt APF system performance subjected to sag and swell disturbances in the PCC voltage

This article has been accepted for publication in a future issue of this journal, but has not been fully edited. Content may change prior to final publication. Citation information: DOI 10.1109/TIE.2020.3031529, IEEE Transactions on Industrial Electronics

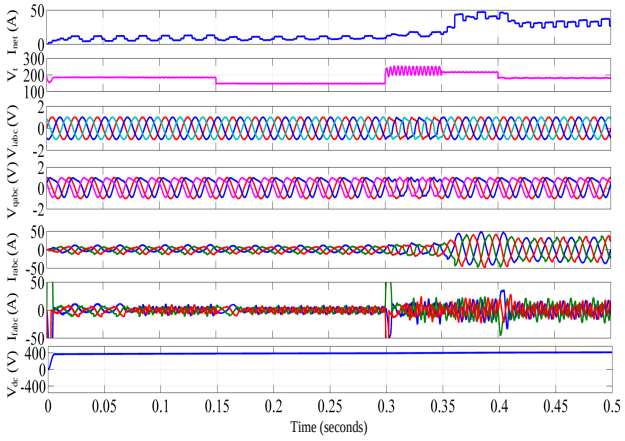

Fig. 8. Control characteristics with various test cases

is also evaluated. In this conditions, we have considered a percentage of 10% of increased and decreased of the nominal grid voltage for the sag swell conditions. According to the dc-link voltage calculation, we have given 375V as a reference voltage. In the grid transient conditions, the Fuzzy tuned PID controller tunes its control gains and maintain the dc-link bus voltage according to the grid voltages which is observed from Fig. 7 from 0.15s to 0.3s the system operates with voltage fall, from 0.3 s to 0.4 s the system operates under a swell/raise condition which is also shown in Fig. 7. In this conditions, the currents of the grid is increasing and decreasing under sag and swell conditions to maintaining the balanced power at the consumer terminals which is observed from Fig. 7. In this condition, the THD content in the phase-A grid current is 2.24%, and 2.32%, respectively.

C. Supply voltages distorted condition

The proposed PV integrated shunt APF system performance subjected to distorted supply voltages in the PCC is also analyzed. In this condition, to validate the controller aggressive behaviour and eliminate the voltage harmonics, we have injected 3^{rd} and 5^{th} harmonics into the grid voltages by using the three-phase programmable source manually. The proposed controller has been extracted fundamental components from the polluted grid voltages and the extracted voltages (V_{sabcf}) are clearly sinusoidal which are shown in Fig. 7 from 0.3s to 0.35s. The Fuzzy tuned PID controller tunes its control gains and maintain the dc-link bus voltage according to the grid voltages which is also observed from Fig. 7. In this condition, the THD content in the phase-A grid current is found good within the IEEE-519 limits.

D. Dynamic load condition

The proposed APF scheme's performance has been performed with increased load condition. In this condition the potency of APF with the proposed technique is performed on simulation platform. The load dynamic state is noticed due to addition and removed of load instantly. In Fig. 7, from 0.35 to 0.5s the system is operating with dynamic load state. To validate the performance during this condition, an additional load is added. The raise in grid current is noticed, which means that the power being injected in the grid. Moreover, the control characteristics are shown in in Fig. 8, where the change in control characteristics are also observed. The harmonic content of the phase-A grid current with the proposed technique in this scenario is has a THD of 2.42%.

V. Experimental Validation

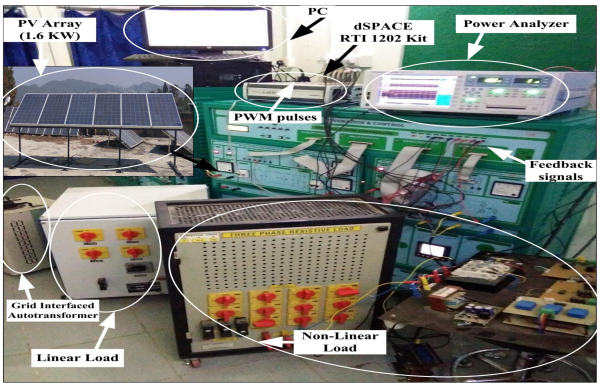

Fig. 9. dSPACE based APF's prototype laboratory setup

To appraise the efficiency of the performance of the MROGI-FLL proposed technique for the APF arrangement, a DS-1202 based experimental platform has been employed. Fig. 9 displays the complete hardware laboratory setup using uncontrolled diode bridge rectifier (acting as nonlinear load) with resistive inductive *(RL)* load, IGBT based bidirectional voltage source inverter (VSI) (25RSB120), HE025T01 Hall-effect current sensor, LV-25 voltage sensor, filter inductor (L_{apf}), dSPACE (DS1202) platform kit, PV simulator (SAS12010), 1.6kW PV panel setup, WT 1800 power quality analyser, Tekronix MDO3024 oscilloscope, Yokogawa-DL850E 8 channel scope-carder, grid emulator, three-phase auto transformer, master computer and scope carder. The system is tested in different states and source current's THD is given in Fig. 21. The proposed technique is based on dc-link voltage regulator and grid interfacing inverter control in the APF. A PWM controller generates required switching signals to the grid interfacing inverter. The APF generate filter currents and injects them into the grid. The parameters taken for the experimental validation are given in Tables I and II respectively.

A. Case 1: Balanced supply voltages condition

By validating the simulation results, PV integrated APF system experimental setup is implemented with the proposed controller which is shown in Fig. 9. The corresponding experimental results are shown in from Fig. 10 to 11. Fig. 10 and 11 shows the grid and proposed control characteristics. The source current THD without the compensation is 26.452% and it is reduced to 2.261% with compensation. Source current is clearly sinusoidal and at unity power factor which is also shown on Fig. 10.

This article has been accepted for publication in a future issue of this journal, but has not been fully edited. Content may change prior to final publication. Citation information: DOI 10.1109/TIE.2020.3031529, IEEE Transactions on Industrial Electronics

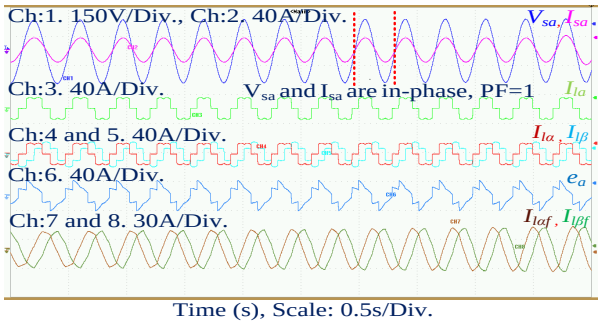

Fig. 10. Grid characteristics under steady-state condition: Ch. 1 and 2: 'A' phase source voltage and current, Ch. 3: 'A' phase load current, Ch. 4 and 5: current α β constituents of the load, Ch: 6, A-phase error current, and Ch: 7 and 8: FCE of the load currents

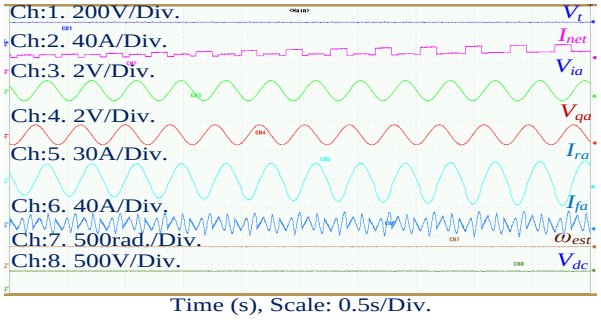

Fig. 11. Control characteristics under steady-state condition: Ch. 1: unit-vector template voltage, Ch. 2: Net-load current, Ch. 3: in-phase voltage component, Ch. 4: quadrature voltage component, Ch. 5: Reference current, Ch. 6: SAPF current, Ch. 7: Estimated frequency and Ch. 8: DC link bus voltage

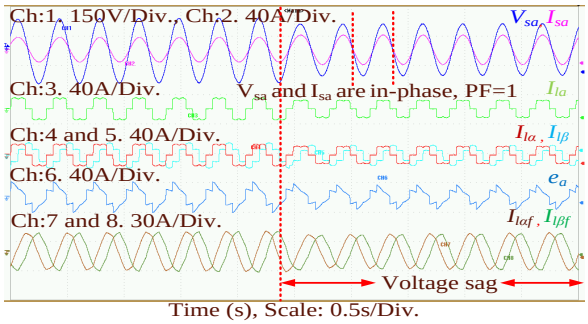

Fig. 12. Grid characteristics under voltage sag condition: Ch. 1 and 2: 'A' phase source voltage and current, Ch. 3: 'A' phase load current, Ch. 4 and 5: current α β constituents of the load, Ch: 6, A-phase error current, and Ch: 7 and 8: FCE of the load currents

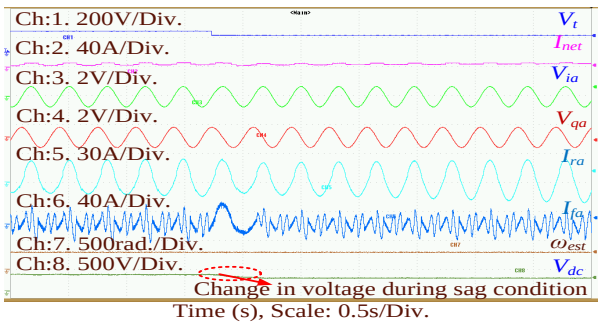

Fig. 13. Control characteristics under voltage sag condition: Ch. 1: unit-vector template voltage, Ch. 2: Net-load current, Ch. 3: in-phase voltage component, Ch. 4: quadrature voltage component, Ch. 5: Reference current, Ch. 6: SAPF current, Ch. 7: Estimated frequency and Ch. 8: DC link bus voltage

B. Case 2 and 3: System voltage sag-swell condition

The proposed PV integrated shunt APF system performance subjected to sag-swell disturbances in the PCC voltage are also evaluated in the experimental platform. In this conditions, we have used a three-phase variac for creating the sag-swell conditions in the grid voltage. According to the dc-link voltage calculation, we have given appropriate reference voltage for sag condition. In the experimental results, the grid current is increased and decreased during voltage sag-swell condition to maintaining the balanced power at the distribution terminals which is observed in Fig. 12 and 14 respectively. Moreover, the Fuzzy tuned PID controller tunes its control gains and maintain the dc-link bus voltage according to the grid voltages and the corresponding control characteristics are observed in Fig. 13 and 15 respectively. The THD content in the phase-A grid current under sag and swell conditions are 2.555% and 2.289% respectively after the SAPF which are shown in Fig. 21.

C. Case 4: Unbalance system voltage condition

The proposed grid-friendly PV connected SAPF system performance subjected to unbalanced voltages in the PCC voltage is also carried out. In this conditions, the magnitude of each phases are changed a percentage of 10% of increased and decreased of the nominal grid voltage for the unbalanced grid voltage conditions by using the three single-phase variacs. Fig. 16 shows the grid voltages, currents, error current and FCE of the load current. At unbalanced grid voltages, the shunt-connected system provides a balanced grid current which is observed from Fig. 16. The proposed control scheme depicts that, the grid-current references are evaluated from average load current multiplied with the unit templates. The average load current and unit templates are constant at any load and grid conditions. The corresponding control results are shown in Fig. 17. The harmonic analysis of this condition is shown

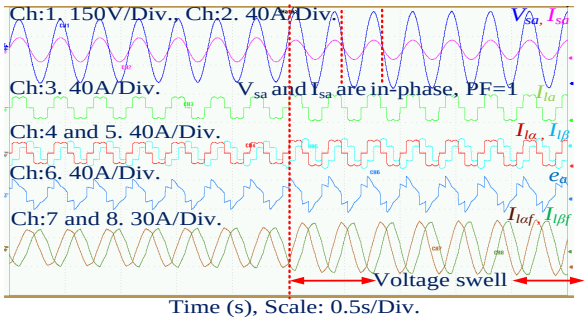

Fig. 14. Grid characteristics under voltage swell condition: Ch. 1 and 2: 'A' phase source voltage and current, Ch. 3: 'A' phase load current, Ch. 4 and 5: current α β constituents of the load, Ch: 6, A-phase error current, and Ch: 7 and 8: FCE of the load currents

This article has been accepted for publication in a future issue of this journal, but has not been fully edited. Content may change prior to final publication. Citation information: DOI 10.1109/TIE.2020.3031529, IEEE Transactions on Industrial Electronics

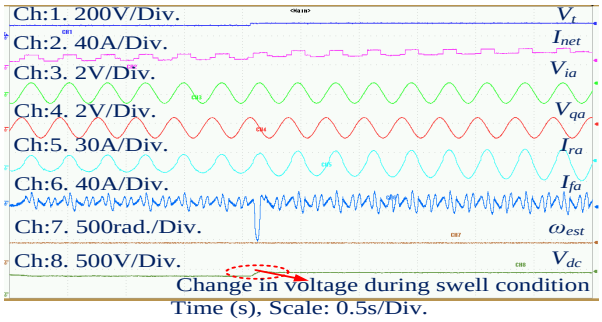

Fig. 15. Control characteristics under voltage swell condition: Ch. 1: unit-vector template voltage, Ch. 2: Net-load current, Ch. 3: in-phase voltage component, Ch. 4: quadrature voltage component, Ch. 5: Reference current, Ch. 6: SAPF current, Ch. 7: Estimated frequency and Ch. 8: DC link bus voltage

in Fig. 21. The source current THD is found satisfactory with in the IEEE-519 limits.

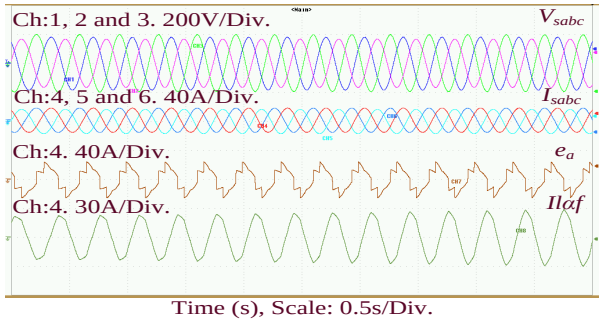

Fig. 16. Grid characteristics under voltage unbalanced condition: Ch. 1, 2 and 3: 'A'-, 'B'- and 'C'-phase source voltages, Ch. 4, 5 and 6: 'A'-, 'B'- and 'C'-phase source currents, Ch. 7: Error current, Ch. 8: FCE of the load current

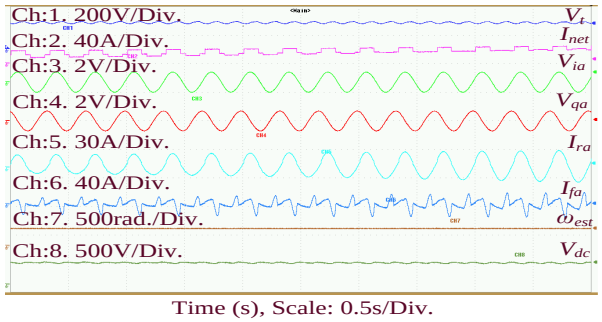

Fig. 17. Control characteristics under voltage unbalanced condition: Ch. 1: unit-vector template voltage, Ch. 2: Net-load current, Ch. 3: in-phase voltage component, Ch. 4: quadrature voltage component, Ch. 5: Reference current, Ch. 6: SAPF current, Ch. 7: Estimated frequency and Ch. 8: DC link bus voltage

D. Case 5: Distorted system voltage condition

As shown in Fig. 18, we have created the source voltage distortion by using the grid emulator. By checking the proposed controller dynamic performance we have created grid voltage distortion. The proposed control algorithm is efficient to remove the harmonics from grid current as well as voltages which are observed from Fig. 18. Fig. 18 shows the grid voltage with harmonics, A-phase grid voltage and current, load current, α β constituents of load current and FCE of load currents respectively. The source current THD in phase-A drops to about 2.586% by using the proposed controller even under a distorted grid voltage condition and power factor is also shows unity which is observed from Fig. 18. The corresponding THD under this condition is shown in Fig. 21 which is under the IEEE-519 limits.

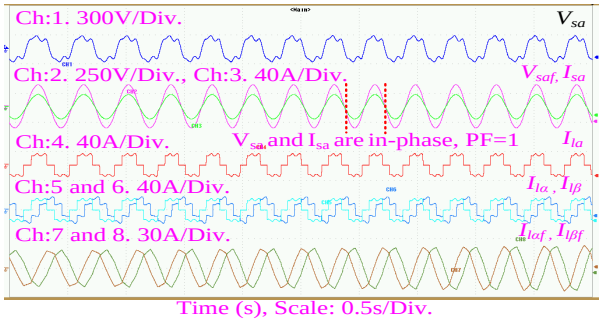

Fig. 18. Grid characteristics under distorted grid voltages condition: Ch. 1: 'A' phase source voltage with harmonics, Ch. 2 and 3: 'A'-phase grid voltage and current, Ch. 4: 'A'-phase load current, Ch. 5 and 6: α β constituents of the load and Ch: 7 and 8: FCE of the load currents

TABLE III
COMPARATIVE STUDY OF PROPOSED CONTROL ALGORITHM WITH EXISTING CONTROL SCHEMES

Characteristics	IRP	SRF	Fryze	Adaline	Proposed
PLL needed	No	Yes	No	No	No
Clark's/Park's transf. needed	Yes	Yes	No	No	No
Steady-state convergence	0.016s	0.022s	0.015s	0.028s	0.021s
THD of grid current (I_{sa})	3.15%	3.58%	3.33%	4.28%	2.162%
FC extraction	NA	NA	NA	NA	Yes
Sampling time	50μs	50μs	50μs	50μs	50μs

E. Case 6 and 7: Load dynamic condition

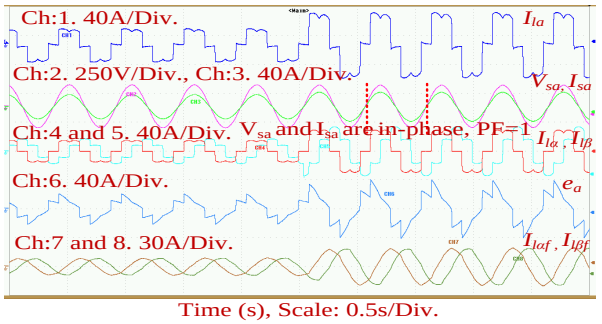

Fig. 19. Grid characteristics under dynamic load condition: Ch. 1: 'A'-phase load current, Ch. 2 and 3: Source voltage and current, Ch. 4 and 5: α β constituents of the load, Ch. 6: 'A'-phase error current and Ch. 7 and 8: FCE of the load currents

Practically systems are heavily subjected to sudden load connection and disconnection. Fig. 19 and 20 shows the proposed SAPF scheme's performance with increased and

This article has been accepted for publication in a future issue of this journal, but has not been fully edited. Content may change prior to final publication. Citation information: DOI 10.1109/TIE.2020.3031529, IEEE Transactions on Industrial Electronics

TABLE IV
COMPARATIVE STUDY OF THE PROPOSED CONTROL ALGORITHM WITH ADAPTIVE CONTROL TECHNIQUES [16-25]

Characteristics	RLS	LMS	LMF	ILST	VSS-LMS	ANF	ESN	ROGI	ISOGI	TOGI	Proposed
Type of filter	Adaptive	Adaptive	Adaptive	Adaptive	Adaptive	Adaptive	Adaptive	Adaptive	Adaptive	Adaptive	Adaptive
Oscillations	moderate	more	high	high	high	moderate	low	low	less	less	very less
Complexity	medium	medium	medium	medium	medium	medium	medium	less	less	less	less
Amplitude tracking	No	No	No	No	No	No	No	good	good	good	Better
Frequency tracking	No	No	No	No	No	No	No	good	good	good	Better
phase angle tracking	No	No	No	No	No	No	No	good	good	good	Better
dc-offset rejection	No	No	No	No	No	No	No	good	Better	Better	Better
FC tracking ability	No	No	No	No	No	No	No	good	Better	Better	Better
Grid synchronisation	No	No	No	No	No	No	No	Yes	Yes	Yes	Yes
Accuracy	good	Moderate	Moderate	Moderate	Moderate	good	good	good	Better	Better	Better
THD of grid currents	2.66%	2.96%	3.3%	2.5%	4%	3.56%	3.25%	3.18%	1.98%	3.8%	2.16%
Sampling time	50μs	50μs	50μs	50μs	50μs	50μs	50μs	50μs	50μs	50μs	50μs
Static error	more	more	more	better	good	good	better	better	small	small	small
Settling time	0.17s	0.1s	0.1s	0.16s	0.15s	0.12s	0.11s	0.1s	0.06s	0.1s	0.05s
Payback time	More	More	More	More	More	More	More	More	Less	Less	Less

TABLE V
COMPARATIVE STUDY OF FUZZY TUNED PID WITH CONVENTIONAL CONTROL SCHEMES

Characteristics	P	PI	PID	FPID
Type of controller	traditional	traditional	traditional	Adaptive
Tuning of gain parameters	Manual	Manual	Manual	Self-tuning
Raise time	High	High	High	Low
Settling time	High	High	High	Low
Dynamic performance	Low	Medium	Good	Better
% of error	High	High	Medium	Very less
Steady-state behaviour	Moderate	Good	Good	Better
Delay time	High	Medium	Moderate	low

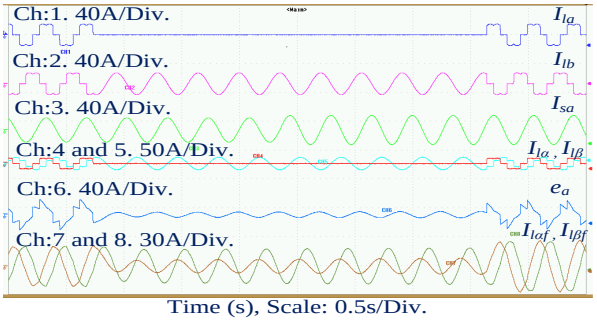

Fig. 20. Grid characteristics under load removed condition: Ch. 1: 'A' phase load current, Ch. 2: 'B' phase load current, Ch. 3: 'A' phase source current, Ch. 4 and 5: α β constituents of the load, Ch. 6: 'A'-phase error current and Ch. 7 and 8: FCE of the load currents

removed load conditions respectively. In this condition, the potency of SAPF with the proposed technique is validated on experimental platform. In this condition, phase-A current of the load has been increased and removed to validating the aggressive behaviour of the proposed control scheme during load transient condition. In Fig. 19, the raise in grid current is observed in the grid current (I_{sa}) with respect to the load current. The PV is giving power to the load continuously when it is balanced load state. After the load increased, both the PV and grid systems are giving power to the load. That is the reason, the grid current is increasing which is observed from Fig. 19. Fig. 20 shows the A-phase load is removed by

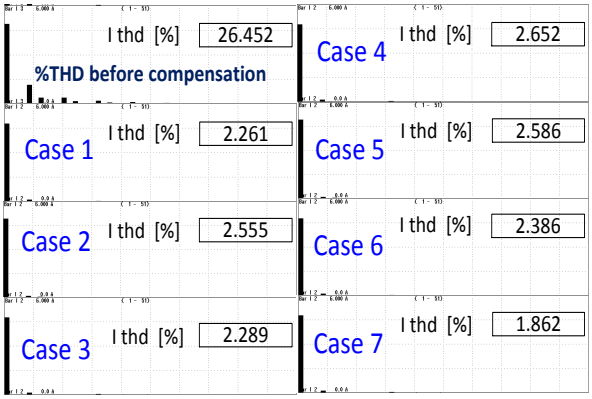

Fig. 21. Real-time THD results under above-mentioned test cases

using the circuit breaker. However, the PV system is giving power to the grid and the load. That is the reason according to which, the phase âbâ current is continuing. If the PV system is not giving power to the load then the remaining phases are not continuing sinusoidal. The experimental THD analysis under these conditions are shown in Fig. 21 which are in found within the IEEE-519 standard limits.

F. Comparative performance of MROGI-FLL technique with existing techniques

Table III displays the comparative performance of proposed system with IRP, SRF technique, Fryze compensation theory, and ADALINE technique based on their characteristics. Table IV summarizes the comparative analysis of proposed technique with RLS, LMS, LMF, ILST, VSS-LMS, ANF, ESN, ROGI, ISOGI and TOGI techniques. Under the steady state and other conditions, the performance of MROGI-FLL technique is found to be best one among of all these techniques. The harmonic analysis of grid current of phase-A with IRP, SRF, ADALINE, and Fryze techniques are shown in Table III. Harmonic spectra of phase-A source currents results in THD of 3.15%, 3.58%, 4.28%, and 3.33%, respectively using these techniques. However, The source current THD using the proposed technique is lower if compared to adaptive techniques. The comparative analyses of proposed technique with

RLS, LMS and LMF, ILST, VSS-LMS, ANF, ESN, ROGI, ISOGI and TOGI techniques are performed under different capabilities. The proposed technique has been found good which is observed from Table IV. Moreover, the comparative analysis of the fuzzy tuned PID with conventional control techniques has also investigated which is given in Table V. The proposed controller's performance is well justified during grid and load transient conditions.

VI. Conclusion

Upon considering the adverse effects of harmonics in a power system network, the MROGI-FLL using APF has been proposed and assessed in this paper. To mitigate current harmonics and for power quality improvement, an adaptive control technique has been developed. The modified ROGI-FLL technique is used to generate the reference currents for APF and a FLPID is utilized for the dc-link voltage control. Along with power quality improvement, pollution-free power generation using PV system has been considered as a key objective. An incremental conductance MPPT controller is used to control the DC-DC converter which maximizes the power yield from the PV system and helps to maintain a stable DC-bus voltage. The proposed MROGI-FLL control strategy appropriately compensates the load and grid harmonics, by adaptively evaluating the amplitude, frequency and phase angle. Moreover, the dynamic performance of the controller has been found satisfactory with very small overshoot and the feed-forward constituent of the PV system is integrated into the control structure to enrich the dynamic behaviour of the system. Simulation results are presented under steady-state, sag-swell condition, load removed condition, distorted grid voltage condition, and dynamic load condition to check the effectiveness of the proposed control strategy. The comparative studies of the proposed control algorithm with already existing and adaptive techniques as IRP, SRF, Fryze, Adaline, RLS, LMS, LMF, ILST, VSS-LMS, ANF, ESN and conventional ROGI, ISOGI and TOGI control techniques are discussed in detail. Finally, the entire system is tested by using a dSPACE based real-time scaled-down prototype and the simulation results are validated. The harmonic analysis in each scenario well adapts to the IEEE-519 standard limits.

References

[1] X. Liang and Ch. Andalib-Bin-Karim, 'Harmonics and Mitigation Techniques Through Advanced Control in Grid-Connected Renewable Energy Sources: A Review', *IEEE Transactions on Industry Applications*, vol. 54, no. 4, pp. 3100-3111, 2018.

[2] P. Acuna, L. MorÃ¡n, M. Rivera, J. Dixon, and J. Rodriguez, 'Improved active power filter performance for renewable power generation systems', *IEEE Transactions on Power Electronics*, vol. 29, pp. 687-694, 2014.

[3] S. K. Khadem, M. Basu, and M. F. Conlon, 'Harmonic power compensation capacity of shunt active power filter and its relationship with design parameters', *IET Power Electronics*, vol. 7, pp. 418-430, 2014.

[4] S. Mikkili, and A. Panda, 'Real-time implementation of PI and fuzzy logic controllers based shunt active filter control strategies for power quality improvement', *International Journal of Electrical Power and Energy Systems*, vol. 43, pp. 1114-1126, 2012.

[5] S. Biricik, S. Redif, O. C. Ozerdem, S. K. Khadem, and M. Basu, 'Real-time control of shunt active power filter under distorted grid voltage and unbalanced load condition using self-tuning filter', *IET Power Electronics*, vol. 7, pp. 1895-1905, 2014.

[6] A. Aithal, and J. Wu, 'Operation and performance of a medium-voltage DC link', *CIRED-Open Access Proceedings Journal*, vol. 2017, no. 1, pp. 1355-1358, 2017.

[7] Z. Wang, F. Zeng, P. Li, C. Wang, X. Fu, and J. Wu, 'Kernel Solver Design of FPGA-Based Real-Time Simulator for Active Distribution Networks', *IEEE Access*, vol. 6, pp. 29146-29157, 2018.

[8] A. K. Panda and R. Patel 'Adaptive hysteresis and fuzzy logic controlled-based shunt active power filter resistant to shoot-through phenomenon', *IET Power Electronics*, vol. 8, no. 10, pp. 1963-1977, 2015.

[9] P. N. Babu, B. Kar and B. Halder, 'Modelling and analysis of a hybrid active power filter for power quality improvement using hysteresis current control technique', *IEEE 7th India International Conference on Power Electronics (IICPE)*, pp.1-6, 2016

[10] S. Zeliang, G. Yuhua, and L. Jisan, 'Steady-State and Dynamic Study of Active Power Filter With Efficient FPGA-Based Control Algorithm' *IEEE Transactions on Industrial Electronics*, vol. 55, no.4, pp.1527-1536, 2008.

[11] P. N. Babu, B. Kar and B. Halder, 'Comparative analysis of a Hybrid active power filter for power quality improvement using different compensation techniques,' *IEEE International Conference on Recent Advances and Innovations in Engineering (ICRAIE)*, pp.1-6, 2016.

[12] M. Qasim, and V. Khadkikar, 'Application of Artificial Neural Networks for Shunt Active Power Filter Control' *IEEE Transactions on Industrial Informatics*, vol. 10, no.3, pp. 1765-1774, 2014.

[13] J. Kanieski, R. Cardoso, H. Pinheiro et al, 'Kalman filter based control system for power quality conditioning devices', *IEEE Transactions on Industrial Electronics*, vol. 60, no. 11, pp. 5214-5227, 2013.

[14] M. A. S. Masoum, S. Jamali, and N. Ghaffarzadeh, 'Detection and classification of power quality disturbances using discrete wavelet transform and wavelet networks', *IET Science Measurement & Technology*, vol. 4, no. 4, pp. 193-205, 2010.

[15] M. A. Platas-Garza and J. A. de la O Serna, 'Polynomial Implementation of the Taylor-Fourier Transform for Harmonic Analysis', *IEEE Transactions on Instrumentation and Measurement*, vol. 63, no. 12, pp. 2846-2854, 2014.

[16] M. Fallah, M. Imani, H. M. Kojabadi, and et al, 'Novel structure for unbalance, reactive power and harmonic compensation based on VFF-RLS and SOGIFLL in three-phase four wire power system', *IEEE Energy Conversion Congress and Exposition (ECCE)*, pp. 6254-6260, 2015.

[17] R. K. Agarwal, I. Hussain, and B. Singh, 'Application of LMS-based NN structure for power quality enhancement in a distribution network under abnormal conditions', *IEEE Transactions on Neural Network & Learning Systems*, vol. 29, no. 5, pp. 1598-1607, 2017.

[18] R. K. Agarwal, I. Hussain, and B. Singh, 'LMF-Based Control Algorithm for Single Stage Three-Phase Grid Integrated Solar PV System', *IEEE Transactions on sustainable energy*, vol. 7, pp. 1379-1387, 2016.

[19] B. Singh, C. Jain, and S. Goel, 'ILST control algorithm of single-stage dual purpose grid connected solar PV system', *IEEE Transactions on Power Electronics*, vol. 29, no. 10, pp. 5347-5357, 2014.

[20] S. Pradhan, I. Hussain, B. Singh, and et al, 'Modified VSS-LMS-based adaptive control for improving the performance of a single-stage PV integrated grid system', *IET Science Measurement & Technology*, vol. 11, no.4, pp. 388-399, 2017.

[21] A. B. Shitole, H. M. Suryawanshi, et al., 'Grid Interfaced Distributed Generation System With Modified Current Control Loop Using Adaptive Synchronization Technique' *IEEE Transactions on Industrial Informatics*, vol. 13, no.5, pp. 2634-2644, 2017.

[22] D. Ali, and R. Abolfazl 'Application of echo state networks for estimating voltage harmonic waveforms in power systems considering a photovoltaic system' *IET Renewable Power Generation*, vol. 11, no. 13, pp: 1688-1694, 2017.

[23] J. Moriano, M. Rizo, E. J. Bueno, R. Martin and F. J. Rodriguez, 'A Novel Multifrequency Current Reference Calculation to Mitigate Active Power Fluctuations,' *IEEE Transactions on Industrial Electronics*, vol. 65, no. 1, pp. 810-818, 2018.

[24] P. N. Babu, B. C. Babu, P. R. Babu and G. Panda, "An optimal current control scheme in grid-tied hybrid energy system with active power filter for harmonic mitigation", *International Trans. on Elect. and Energy Sys.*, vol. 30, no.3, e12183, DOI: 10.1002/2050-7038.12183, 2020.

[25] H. Du, Q. Sun, Q. Cheng, D. Ma and X. Wang, 'An Adaptive Frequency Phase-Locked Loop Based on a Third Order Generalized Integral', *energies, mdpi*, vol. 12, no. 309, doi:10.3390/en12020309, 2019.

[26] S. G. Jorge, C. A. Busada, and J. A. Solsona, 'Frequency adaptive discrete filter for grid synchronization under distorted voltages,' *IEEE Transactions on Power Electronics*, vol. 27, no. 8, pp. 3584-3594, 2012.

This article has been accepted for publication in a future issue of this journal, but has not been fully edited. Content may change prior to final publication. Citation information: DOI 10.1109/TIE.2020.3031529, IEEE Transactions on Industrial Electronics

[27] S. Golestan, J. M. Guerrero, J. Vasquez, A. M. Abusorrah, and Y. A. Al-Turki, 'A study on three-phase FLLs,' *IEEE Transactions on Power Electronics*, vol. 34, no. 1, pp.213-224, 2019.
[28] E. Guest and N. Mijatovic, 'Discrete-time complex band pass filters for three-phase converter systems', *IEEE Transactions on Industrial Electronics*, vol. 66, no. 6, pp. 4650-4660, 2019.
[29] S. Golestan, J. M. Guerrero and J. C. Vasquez, 'Is Using A Complex Control Gain in Three-phase FLLs Reasonable?', *IEEE Transactions on Industrial Electronics*, Early Access, 2019.
[30] P. N. Babu, P. R. Babu and G. Panda, 'An Adaptive Differentiation Frequency based Advanced Reference Current Generator in Grid-tied PV Applications', *IEEE Journal of Emerging and Selected Topics in Power Electronics*, Early Access, Aug-2019.
[31] I. Sefa, N. Altin, S. Ozdemir, and O. Kaplan, 'Fuzzy PI controlled inverter for grid interactive renewable energy systems', *IET Rene. Power Gene.*, vol. 9, no. 7, pp. 729-738, 2015.
[32] X. Quan, X. Dou, Z.Wu, M. Hu, and A. Q. Huang, 'Complex-coefficient complex-variable filter for grid synchronization based on linear quadratic regulation,' *IEEE Transactions on Industrial Informatics*, vol. 14, no. 5, pp. 1824-1834, May. 2018.
[33] B. Singh, A. Chandra and K. Al-Haddad, 'Power Quality: Problems and Mitigation Techniques,' *Wiley book publisher*, ISBN: 978-1-118-92208-8, Dec-2014.

N arendra Babu P received the B.Tech. degree in electrical and electronics engineering from JNTU, Hyderabad, India, and the M.Tech. degree in power and energy systems specialization from the National Institute of Technology Meghalaya, Shillong, India, in 2010 and 2017, respectively. He is currently a Senior Research Fellow (SRF) with RECTPCL-CSR Funded Project and Ph.D. Research Scholar, Department of Electrical Engineering, National Institute of Technology Meghalaya, Shillong, India. His current research interests include renewable energy technologies, hybrid ac-dc Microgrid, Power Quality and control of grid-tied inverters.

J osep M. Guerrero (S'01-M'04-SM'08-FM'15) received the B.S. degree in telecommunications engineering, the M.S. degree in electronics engineering, and the Ph.D. degree in power electronics from the Technical University of Catalonia, Barcelona, in 1997, 2000 and 2003, respectively. Since 2011, he has been a Full Professor with the Department of Energy Technology, Aalborg University, Denmark, where he is responsible for the Microgrid Research Program. From 2014 he is chair Professor in Shandong University; from 2015 he is a distinguished guest Professor in Hunan University; and from 2016 he is a visiting professor fellow at Aston University, UK, and a guest Professor at the Nanjing University of Posts and Telecommunications. From 2019, he became a Villum Investigator by The Villum Fonden, which supports the Center for Research on Microgrids (CROM) at Aalborg University, being Prof. Guerrero the founder and Director of the same centre (www.crom.et.aau.dk).
His research interests is oriented to different microgrid aspects, including power electronics, distributed energy-storage systems, hierarchical and cooperative control, energy management systems, smart metering and the internet of things for AC/DC microgrid clusters and islanded minigrids. Specially focused on microgrid technologies applied to offshore wind, maritime microgrids for electrical ships, vessels, ferries and seaports, and space microgrids applied to nanosatellites and spacecrafts. Prof. Guerrero is an Associate Editor for a number of IEEE TRANSACTIONS. He has published more than 600 journal papers in the fields of microgrids and renewable energy systems, which are cited more than 50,000 times. He received the best paper award of the IEEE Transactions on Energy Conversion for the period 2014-2015, and the best paper prize of IEEE-PES in 2015. As well, he received the best paper award of the Journal of Power Electronics in 2016. During seven consecutive years, from 2014 to 2020, he was awarded by Clarivate Analytics (former Thomson Reuters) as Highly Cited Researcher with 50 highly cited papers. In 2015 he was elevated as IEEE Fellow for his contributions on "distributed power systems and microgrids."

P ierluigi Siano (M'09-SM'14) received the M.Sc. degree in electronic engineering and the Ph.D. degree in information and electrical engineering from the University of Salerno, Salerno, Italy, in 2001 and 2006, respectively.
He is a Professor and Scientific Director of the Smart Grids and Smart Cities Laboratory with the Department of Management & Innovation Systems, University of Salerno.
His research activities are centered on demand response, on energy management, on the integration of distributed energy resources in smart grids, on electricity markets and on planning and management of power systems.
In these research fields he has co-authored more than 500 articles including more than 300 international journal papers that received in Scopus more than 9450 citations with an H-index equal to 47.
He received the award as 2019 Highly cited Researcher by ISI Web of Science Group. He has been the Chair of the IES TC on Smart Grids.
He is Editor for the Power & Energy Society Section of IEEE Access, IEEE TRANSACTIONS ON INDUSTRIAL INFORMATICS, IEEE TRANSACTIONS ON INDUSTRIAL ELECTRONICS, Open Journal of the IEEE IES and of IET Renewable Power Generation.

R angababu Peesapati (M'14) received the Ph.D. degree in electronics science from the University of Hyderabad, Hyderabad, India, in 2014. Since 2014, he has been an Assistant Professor in the Department of Electronics and Communication Engineering, National Institute of Technology Meghalaya, Shillong, India. His research interests include design of FPGA-based reconfigurable systems for multimedia, signal processing, and evolutionary computing.

G ayadhar Panda (M'07-SM'19) received the B.E. degree in electrical engineering from the Institute of Engineers, Kolkata, India, in 1996, the master's degree in power electronics from Bengal Engineering College (presently IIEST), Shibpur, India, in 1998, and the Ph.D. degree in electrical engineering from Utkal University, Bhubaneswar, India, 2007. He is currently a Professor with the Electrical Engineering Department, National Institute of Technology, Meghalaya, India. He has served as Head of the department and Chairman of various committees at institute level. He is also currently looking after Dean academic affairs (AA) at NIT Meghalaya. He has published more than 80 technical papers in national and international conferences proceedings or journals. He has more than 20 years of teaching experience.
His current research interests include automatic generation control, stability improvements using flexible alternating current transmission system devices, power quality, power electronic converters, and distributed power generation.